Variability in sliding behaviour of carbon fibre tows investigated by Discrete Element Method and experiments

Olga Smerdova, Chenghao Chai, Ismail Kolimi, Noël Brunetière

Composites: Part A 193 (2025) 108818

Contents lists available at ScienceDirect

Composites Part A

journal homepage: www.elsevier.com/locate/compositesa

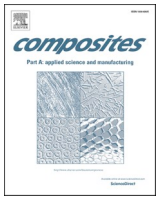

Variability in sliding behaviour of carbon fibre tows investigated by Discrete Element Method and experiments

Olga Smerdova *, Chenghao Chai, Ismail Kolimi, Noël Brunetière

Institut Pprime (UPR 3346 CNRS/ISAE-ENSMA/UNIVERSITÉ DE POITIERS), Department of Physics and Mechanics of Materials, 1 Avenue Clement Ader, BP 40109, Futuroscope, 86961 Cedex, France

HIGHLIGHTS

- Sliding behaviour of carbon fibre tow is simulated with a Discrete Element Model.
- Variability in experimental results is explained by numerical parametric study.
- Torsional and bending stiffnesses of fibres have the highest impact on tow sliding.
- Fibre/fibre and fibre/tool friction coefficients impact tow sliding only slightly.
- Accommodation of sliding behaviour with cycles is observed.

GRAPHICAL ABSTRACT

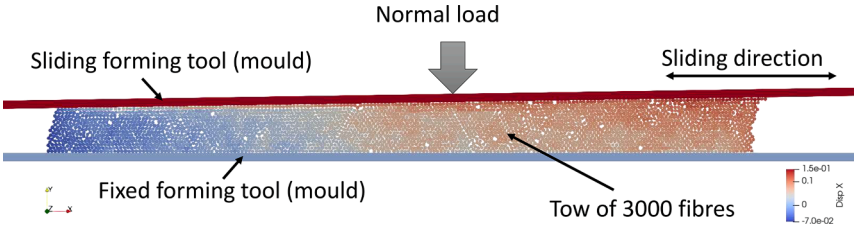

1. Introduction

Sliding friction of raw composite plies or bands under some kind of pressure is ubiquitous in all manufacturing processes for composite materials requiring a tool or a mould, which excludes only additive manufacturing. Although a large number of manufacturing processes exist, four moulding techniques – layup, injection moulding, compression moulding, and resin transfer moulding – share more than ¾ of the global market for composite materials [1].

From a tribological point of view, the manufacturing processes of composite materials can be grouped into two families depending on whether the sliding contact of fibre reinforcement is lubricated by liquid polymer or not. In some processes, such as compression moulding, hand or automated layup, vacuum or diaphragm moulding, the fibre reinforcement is first impregnated with resin and then moulded into a desired shape. The curing of the resin occurs under heating and/or pressure. In other processes, such as simple or vacuum-assisted resin transfer moulding or injection moulding, a dry preform composed of fibre mats or woven fabrics is shaped prior to impregnating it with polymer. A first advantage of the second family of processes is that they do not require the manufacturing of a semi-product mixed with resin, which reduces the cost and the environmental impact. A second and major advantage is that parts of complex shape and variable size can be manufactured with accuracy from unidirectional stitched cloths or woven fabrics and a variety of polymer matrices. Indeed, there has been a growing pressure to replace thermosetting polymer matrices with thermoplastic polymers due to recyclability issues. However, the processing of thermoplastic matrices usually requires high pressure due to high polymer melt viscosity, which means that these polymers cannot be used in all processes cited above [2]. More recently, the processes traditionally used with thermosetting resins, such as low pressure or vacuum infusion and resin transfer moulding, have been successfully employed with reactive thermoplastic polymers [3,4].

In both types of processes, the sliding between the composite material and the mould plays a crucial role and conditions the final shape and quality of the part. That is why a number of researchers have been

* Corresponding author.
E-mail address: olga.smerdova@ensma.fr (O. Smerdova).

https://doi.org/10.1016/j.compositesa.2025.108818
Received 17 January 2025; Received in revised form 14 February 2025; Accepted 19 February 2025
Available online 25 February 2025

studying the friction of composite semi-products. However, since the composite materials are multiscale, the approaches to study this friction also differ depending on the considered scale: macroscopic ply on tool or ply on ply friction [5–8], mesoscopic tow on tool or tow on tow friction [9–15], and microscopic fibre on tool or fibre on fibre friction [16–19]. Each scale matters since they are interdependent. To understand and model the friction between plies correctly, which is responsible for the correct global shape of the part, it is necessary to consider smaller scales. The friction at the scale of a tow is responsible for local sliding defects in the final part, which can have a crucial impact on the mechanical properties of the part.

It was highlighted by Potter et al. [20] that some variability in composites is inevitable due to design and cannot be attributed to poor manufacturing. However, there are also a number of defects that can be avoided by improving the process. Hamidi and Altan [21] reviewed the defects in composites produced by resin transfer moulding methods. Among them, the dry preform defects, which are of interest for the present study, refer to irregularities of reinforcement path and geometry. These are fibre misalignments and in-plane and out-of-plane undulations, called wrinkles and waviness. It is the latter that induces the highest loss of mechanical properties in final parts that can reach a 70 % reduction in flexural strength [20], 70 % in the elastic modulus, and a 15-year reduction in fatigue life [21,22]. These defects have been observed in woven as well as in non-crimp fabric preforms. In particular, Viisainen and Sutcliffe [23] found that some variability in these defects comes from inter-ply friction. On the other hand, Guzman-Maldonado et al. [24] and Boisse et al. [25] revealed by experiments and modelling that the two main causes of wrinkles are quasi-inextensibility of fibres and slippage between them.

The friction of fibres and tows was studied previously in a number of experimental works. Although it is natural to expect that the slippage behaviour of these long, thin, and flexible fibres is related to their bending and torsional stiffness, which in turn are dependent on the boundary conditions and, in particular, axial tension, this dependency has never been investigated. Unfortunately, it is impossible to control the axial tension of each fibre accurately when it is applied to a tow composed of thousands of fibres. In this context, the first aim of the present work was to design and conduct an experiment that highlights the variability of the sliding response of a tow in terms of frictional force, its sliding displacement, and its transversal strain under compressive and shear load imposed by a smooth tool. To understand and explain this variability, the second and main aim of this work was to develop a simple numerical model of a sliding tow and to conduct a parametric study of varying mechanical and frictional parameters of the fibres. The effects of the tow shape, the number of cycles of sliding, and the compressive load were also studied to help adjust manufacturing processes with respect to this sliding behaviour and to attempt to better control the appearance of the defects in final composite products. A

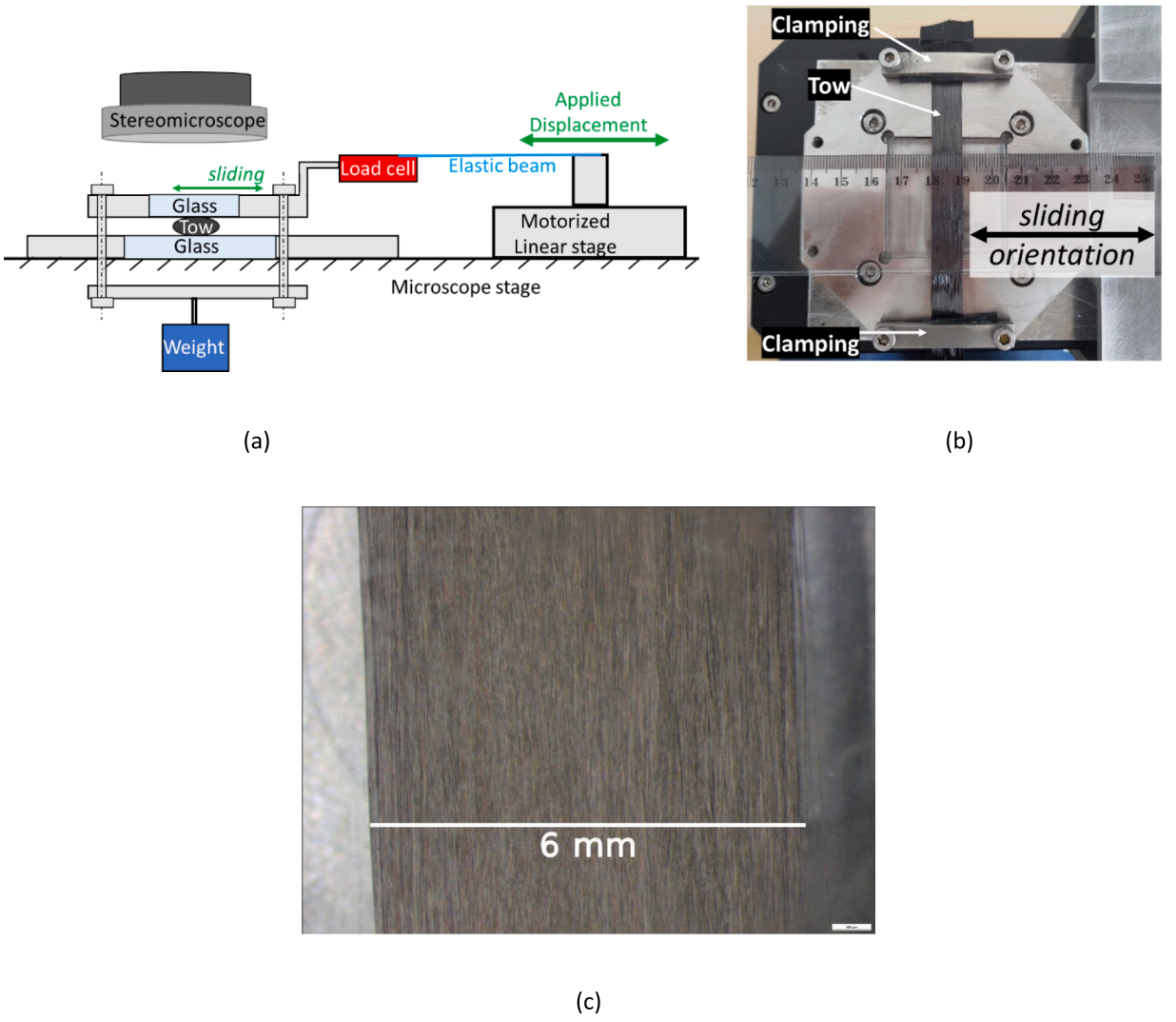

Fig. 1. (a) Schematic drawing of the experimental setup, (b) tow fixed on the stage and (c) microscopic image of the carbon fibre tow through the glass window.

Discrete Element Method, implemented with the open-source software LMGC90 developed at the University of Montpellier by Moreau [26] and Jean [27], was chosen to create this model since it enables simulations of a large number of interacting bodies with a low computational cost.

2. Materials and experiments

Sliding experiments were carried out on T700SC-12 k-60E carbon fibre tow with an average diameter of carbon fibres of 6.7 μm, a small amount of sizing to enhance compatibility with epoxy, and 12,000 fibres in a tow. Several pieces of tow were cut from the same spool and handled and tested in the same way. The experimental set-up to study the sliding of carbon fibre tow was already described elsewhere [28,29]. This home-made tribometer, schematised in Fig. 1(a), is equipped with a force sensor to measure small friction forces in the sliding contact between the carbon tow, which can be fixed in different orientations with respect to the sliding direction, and the moving glass plate under a constant normal weight of 6.55 N. The weight is applied through a mass suspended under the sliding plate. Fig. 1 (b) presents the tow as it was used in the present study, clamped at two edges with a distance of 100 mm between them and positioned transversely to the sliding orientation. The axial tension of the tow, 4.9 N nominally, is applied by suspending a weight of 500 g to a free end of the tow while the other end is clamped. The second end is then clamped by screwing a rubber/aluminum part to the bottom plate, as seen in Fig. 1 (b) and the weight is removed. Due to the small size of the tribometer, it is possible to place it under a microscope or a camera to observe the contact through the glass plate during sliding. A previous paper using this setup [28] focused on the correlations between the three-dimensional shape of the tow after incremental sliding, measured with a 3D optical microscope, and the friction signal. The results presented in the current paper were obtained in a slightly different configuration. Firstly, the manual micrometric screw used to apply the sliding to the upper part of the tribometer was replaced by a linear stage. This permitted the application of a constant sliding speed and minimised the human factor in the obtained data. The stage was MFA-CC from Newport equipped with a DC motor. This stage offers a precise motion of linear trajectory with minimal incremental motion of 1 μm and a maximum run of 25 mm. Secondly, in the work presented here, the tribometer was placed under an optical stereomicroscope in order to observe the whole width of a tow at once and to be able to record images during the sliding of a tow. A stereomicroscope Zeiss Discovery.V12 was used with an objective of x8. The video files of sliding were recorded with a frequency of 5 images per second.

The images from the stereomicroscope, such as the one presented in Fig. 1(c), were then analysed with a Matlab routine to detect the edges of the tow and to deduce the tow displacement and its transversal strain at

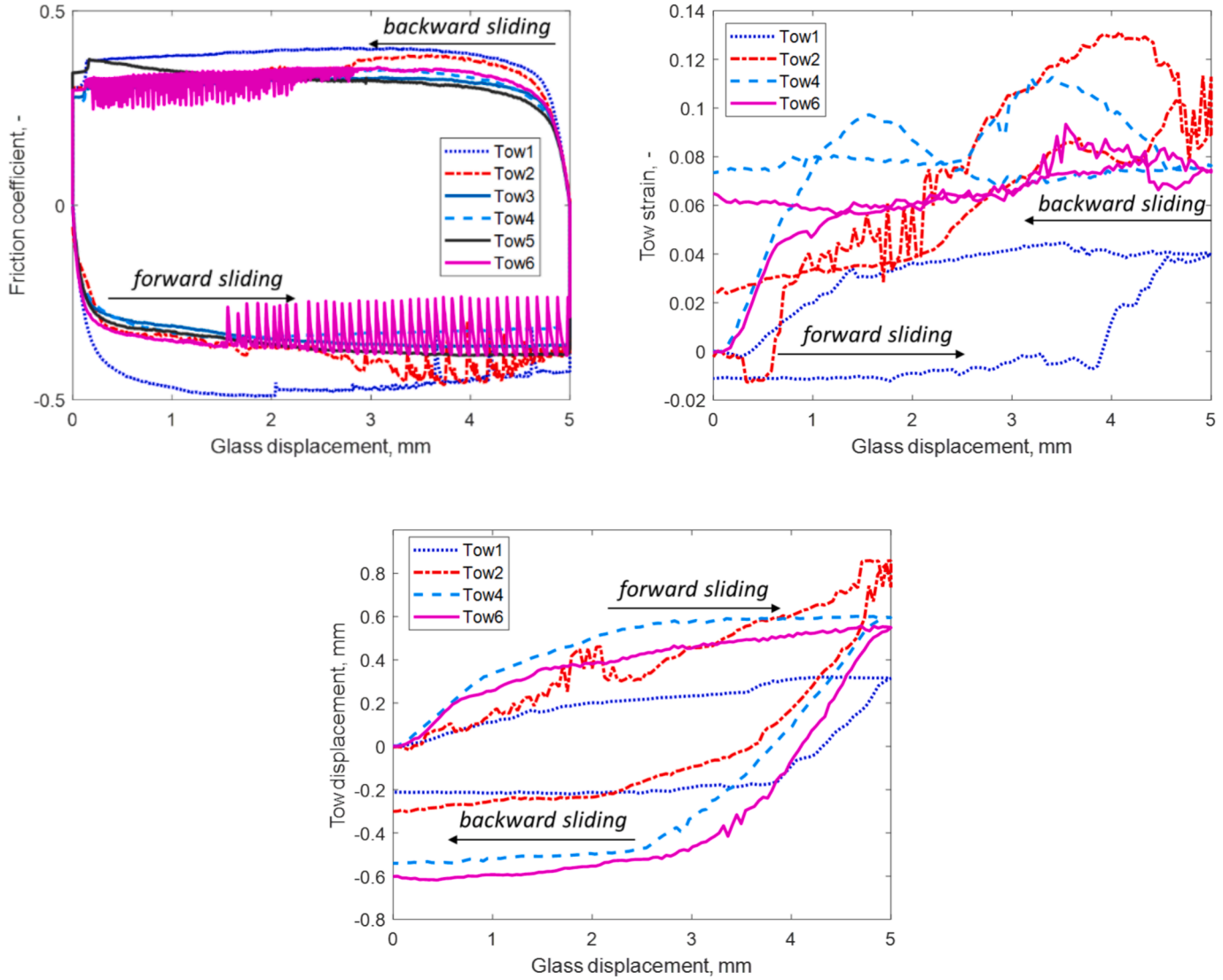

Fig. 2. Experimentally measured friction coefficient, tow strain and tow displacement as a function of the displacement of the sliding glass.

each time step. The displacement of the centre of the tow d_T is computed as the relative position of the 2D centroid of the black tow in the white microscope image compared to the initial image before sliding. The Hencky strain ε_T of the tow is computed as

$$\varepsilon_T(t) = \ln \frac{w_T(t)}{w_T(t_0)} \tag{1}$$

where $w_T(t)$ is the width of the tow as a function of time and t_0 is the reference time after compression but before the beginning of sliding. The instantaneous friction coefficient $\mu(t)$ is calculated as a ratio of the friction force constantly measured during sliding by the load sensor and the constant normal load applied by the weight.

Four sliding cycles of 5 mm of sliding distance with a sliding speed of 0.1 mm/s were applied to most of the tows. The sliding speeds of 1 mm/s and 0.01 mm/s were also tested, but no significant difference in the results was recorded.

The results presented in Fig. 2 were obtained during the first sliding experiment, right after the compression of the tow. The friction coefficient, displacement of the tow, and tow strain are presented as a function of the sliding distance of the glass during the first cycle of sliding. Six friction experiments, with four of them under the stereomicroscope, demonstrate rather significant variability in response. This is not very surprising given the manual handling of the tows and their highly deformable nature. The dispersion in the initial width of these tows was between 6.5 and 8.8 mm. In some tests, the tow separated into two parts during the forward pass and rearranged together during the backward pass. The movements of individual fibres were also visible in the images, but the resolution was not sufficient to analyse them quantitatively. It appeared, for instance, that some tows also separated into layers and the top layer slid on the bottom layer for some distance.

The friction signal is smooth in some tests, while other tests present some instabilities that could be attributed to the stick–slip behavior of the contact. This type of behavior is usually controlled by the stiffness of the system, its mass and the sliding speed. Since the sliding speed and the mass were identical in all tests, the observed vibrations are probably due to the difference in the stiffness of the tows. The average friction coefficient at the last 50 % of sliding was 0.38 ± 0.036 in the forward pass and 0.33 ± 0.019 in the backward pass. The displacement of the tow after one pass is 0.58 ± 0.149 mm, and after the return, it is -0.42 ± 0.155 mm. Finally, the strain of the tow is 0.07 ± 0.015 and 0.04 ± 0.029 with one tow finishing the cycle in a compressed state and the three others in a stretched one.

3. Numerical model

3.1. Discrete Element Method

In contrast to the Finite Element Method (FEM), which is classically used to model continuum mechanics problems, the Discrete Element Method (DEM) deals with interactions of a large number of particles. The DEM was initially developed to simulate the mechanics of granular geological materials [30]. In these numerical simulations, a set of motion and contact equations is solved iteratively for the whole assembly of rigid and usually spherical particles. Due to the development of cohesive interaction laws, the DEM has later been successfully used to simulate continuum mechanics problems with local discontinuities, like brittle fracture, impact, or wear of homogeneous and heterogeneous materials [31,32].

In the classical so-called smooth contact particle methods, there is only one contact between each pair of particles, and interpenetrations are allowed. In the first step of computation, the interaction forces are computed based on the interpenetrations. In the second and last step, Newtonian dynamics is applied to find new velocities and positions of the particles. These iterations are repeated until the end of the simulation. The algorithm used in this work is based on a different formulation of the DEM, called the Non-Smooth Contact Dynamics Method [26,27,32,33]. The interpenetration is prohibited and, instead, a dry Signorini contact law with Coulomb friction governs the contacts between particles. An iterative process is used to compute forces and velocities of all particles until a convergence criterion is fulfilled.

The work presented in this paper has been numerically implemented using the LMGC90 open-source software [34] developed at the University of Montpellier, France. LMGC90 uses the Non-Smooth Contact Dynamics Method with implicit time integration (theta method). The contact solver used by the software is Stored Delassus Loops with the Non-Linear Gauss Seidel algorithm.

3.2. Model of the carbon fibre tow

Since the friction tests are conducted on the central part of fibres that are much longer (100 mm), it can be assumed that this is a plane strain problem. Therefore, a two-dimensional approach will be adopted. Some 3D effects, resulting from the fact that the fibres are not perfectly aligned, cannot be captured by the 2D model, where the fibres are assumed to be parallel. However, the computational cost of solving a full 3D problem is too high for a parametric study like the one presented in this paper.

The reference model is constituted of 3,000 circular particles representing the cross-section of the fibers in the middle of the tow and 1,000 ghost particles inserted at the beginning of the simulation in order to create voids in the tow cross-section. These ghost particles disappear from the beginning of the compression, leaving the fibres to take their place. The radii of the fibres are generated as a random normal distribution with a mean value of 3.45 μm and a standard deviation of 0.125 μm. These values are taken from the experimental work of [35], who measured the diameters of T700 carbon fibres and provided the statistics. The radii of the ghosts are taken as between 7.5 and 11 μm arbitrarily. The particles are shuffled and deposited in a rectangular box of 1.2 mm x 0.4 mm (300 x 100 Rmax) using the deposit function of LMGC90 code by minimising the gravitational potential.

The two glass plates are modeled as rectangular bars of 2.9 mm x 16 μm. One bar is beneath the box of fibres, just in contact, and the other one is on the top of the box at 0.4 mm. Since the box is not fully filled, there is a small space of about 20 μm between the top fibres and the upper plate initially. The bottom plate is horizontally aligned with the middle of the tow, and the top plate is shifted horizontally from the middle of the tow to the left by 0.2 mm. A schematic drawing of the model with some characteristic dimensions is presented in Fig. 3.

Both particles and plates are modeled as rigid bodies with a density of 0.0001 g/mm3 (0.1 g/cm3) and 0.0025 g/mm3 (2.5 g/cm3), respectively. Note that the density of the fibres has no effect on the results because of the low speed, so a low (not realistic) value of the density was chosen to reduce computation time and improve convergence.

In 2D space, there are three degrees of freedom (DoF): horizontal (u_x) and vertical (u_y) displacements and in-plane rotation (θ_z). For the bottom plate, the three DoF are fixed. The upper plate is under imposed vertical force and horizontal speed, and its rotation is not restricted, as in the experiments where the top plate is attached to an elastic beam allowing tilt. Firstly, a load is applied onto the top plate, calculated as the average experimental normal pressure multiplied by the width of the box: $0.046MPa \times 1.2mm = 0.055N/mm$. This load is applied as follows: from 0 to 0.5 s, the top plate falls under gravity only; then, from 0.5 to 1 s, the normal load increases exponentially up to the maximum value. After one second, the normal load remains constant, and the top plate starts to move horizontally with the prescribed speed. From 1 s to 3 s, the speed is 0.2 mm/s; then it becomes 0 mm/s for 0.5 s, and then the plate comes back with the speed of −0.2 mm/s for 2 more seconds. The whole experiment of 1 cycle of sliding, including the compression phase, lasts 5.5 s.

The movements and rotations of the particles representing fibres are

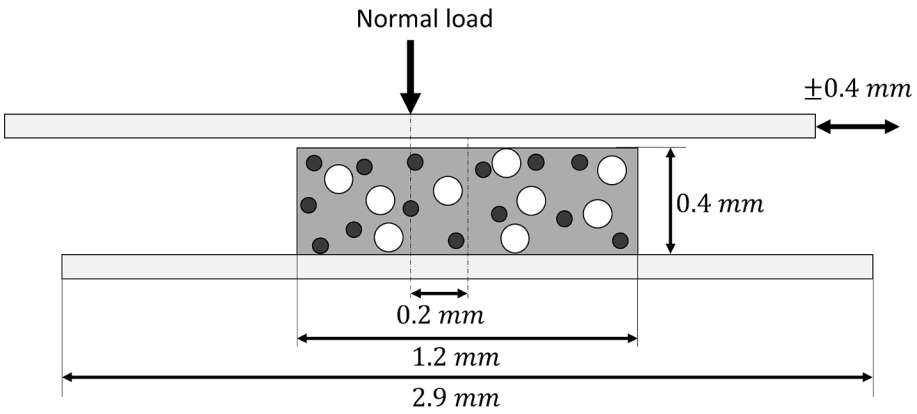

Fig. 3. Schematic drawing of the initial configuration of the model with dimensions. White and dark circles represent respectively voids and fibres.

restricted by linear springs accounting for the third dimension of the fibres. Indeed, since the fibres are very long (100 mm) compared to their diameter (6.9 μm on average), the movement of the section of each fibre is controlled by its bending, and the rotation is governed by its torsion. The torsional stiffness of a carbon fibre was roughly estimated with the Euler-Bernoulli double-clamped beam model using the shear modulus in torsion measured by [36]. The authors measured the torsional modulus, G, between 22 and 25 GPa for high modulus and high strength fibres, respectively. The torsional stiffness of a fibre k_T [Nm/rad] is defined as

$$k_T = \frac{M_T}{\theta} = \frac{GJ}{L/2} \tag{2}$$

where θ is the rotational angle of a fibre in rad. With the length of a fibre $L = 100mm$, its diameter $d = 7 \times 10^{-3}mm$, the torsional moment of area $J = \frac{\pi d^4}{32} = 235\mu m^4$, the $k_T = 1.2 \times 10^{-10}Nm = 1.2 \times 10^{-7}Nmm$.

To estimate the bending stiffness of the fibres, a simple 2D FE model of a beam with nonlinear behavior was used. The relation between the bending stiffness of a fibre and its axial load was found to be linear, with a coefficient of proportionality of 0.043 mm^{-1} for the axial load in the range of 4.17×10^{-6} to 4.17×10^{-3} N. These results were used in the LMGC90 simulation to explore the effect of the bending stiffness of fibres k_b, which was chosen between 2.7×10^{-7} and 1.8×10^{-4} N/mm.

Torsional moment M_T and bending forces F_x and F_y were applied to each fibre at the beginning of each computation step as spring forces proportional to the relative displacement and rotation of the particle. The bending and rotational stiffness are constant during the simulation and are similar for all particles. However, different k_{bX} and k_{bY} values are used to account for differences in compression and sliding behavior. The contact between the particles and the walls is governed by an inelastic quasi-shock contact law coupled with Coulomb's friction law. Two distinct coefficients of friction are used in the carbon fiber tow model: the friction between carbon fibers (μ_{ff}) and the friction between a fiber and a glass plate (μ_{fgl}). The static forces acting on each fiber are illustrated in Fig. 4.

The model developed using the aforementioned procedure was employed to conduct a parametric study aimed at understanding the impact of various parameters on the sliding behavior of the tow. Specifically, the study examined the following factors: the fiber/fiber friction coefficient (μ_{ff}), the fiber/glass friction coefficient (μ_{fgl}), vertical bending stiffness(k_{bY}), horizontal bending stiffness (k_{bX}), torsional stiffness (k_T), the number of particles, the normal load applied to the sliding glass, and the shape of the box filled with fibers, as detailed in Table 1. The results from these 19 simulations, along with two additional simulations involving repeated sliding cycles (each repeated four times), are presented and discussed in the following section. Each simulation of a sliding cycle required approximately 4 h of computation time. Convergence was verified after each simulation, and the maximum

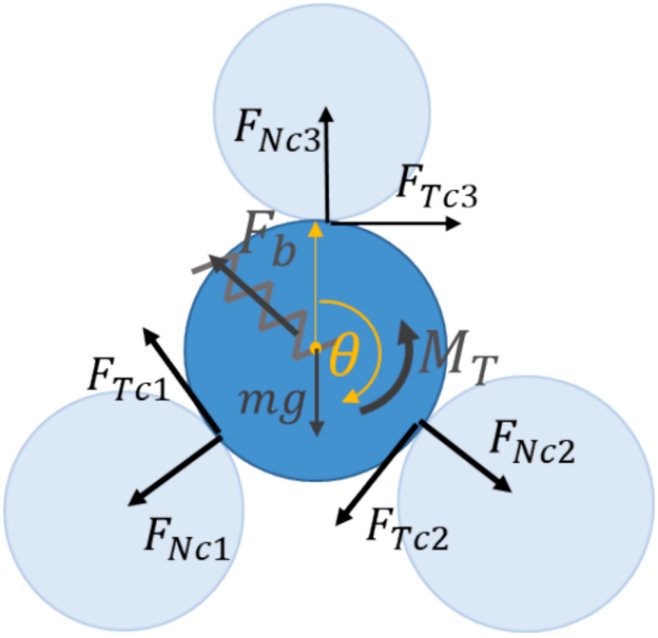

Fig. 4. Free body diagram of a fibre in a tow.

number of iterations was set to 25,551, which was sufficient to ensure convergence at all steps.

4. Results and discussions

The thickness of the tow under compression was measured in our previous paper [29] using a 3D microscope. It ranged from 100 to 300 μm, depending on the width of the tow. This corresponds to a thickness of 14 to 42 fibers. In the reference model, the thickness and width of the tow after compression were 108 μm and 1.259 mm, respectively. For the models with the same initial box, these values did not vary by more than 11 μm for thickness and 125 μm for width. This thickness is at the low end of the experimental values, but it represents a compromise between the number of fibers and the width of the tow. Indeed, the DEM tow is likely denser than the real tow. The particles in the two-dimensional model are subject to the gravity and normal load of the glass, and each particle must rely on either another particle or the glass bottom plate. In contrast, in the real tow, the fibers are not perfectly aligned, leaving spaces between the fibers in each cross-section [12]. Therefore, the model with 12,000 fibers (N19) is only 113 μm thick and 4.828 mm wide.

Table 1
The values of the variable parameters for all simulations. The value different from the reference configuration is bold and underlined.

Simulation	Frictional parameters		Structural parameters			Number of particles	Normal load, N/mm	Initial size of the box, mm^2
	μ_{ff}	μ_{fgl}	$k_{bX}, N/mm$	$k_{bY}, N/mm$	k_T, $N\ mm$			
N1 (Ref)	0.1	0.35	10^{-4}	10^{-6}	10^{-7}	3000	−0.055	1.2 x 0.4
N2	0.1	0.35	10^{-4}	10^{-6}	10^{-7}	3000	−0.055	1.2 x 0.4
N3	0.1	0.35	10^{-4}	10^{-6}	10^{-7}	3000	−0.055	1.2 x 0.4
N4	***0.3***	0.35	10^{-4}	10^{-6}	10^{-7}	3000	−0.055	1.2 x 0.4
N5	***0.5***	0.35	10^{-4}	10^{-6}	10^{-7}	3000	−0.055	1.2 x 0.4
N6	0.1	***0.5***	10^{-4}	10^{-6}	10^{-7}	3000	−0.055	1.2 x 0.4
N7	0.1	***0.7***	10^{-4}	10^{-6}	10^{-7}	3000	−0.055	1.2 x 0.4
N8	0.1	0.35	10^{-4}	10^{-6}	$\boldsymbol{10^{-8}}$	3000	−0.055	1.2 x 0.4
N9	0.1	0.35	10^{-4}	10^{-6}	$\boldsymbol{10^{-6}}$	3000	−0.055	1.2 x 0.4
N10	0.1	0.35	10^{-4}	10^{-6}	***inf***	3000	−0.055	1.2 x 0.4
N11	0.1	0.35	$\boldsymbol{10^{-5}}$	10^{-6}	10^{-7}	3000	−0.055	1.2 x 0.4
N12	0.1	0.35	10^{-4}	$\boldsymbol{10^{-5}}$	10^{-7}	3000	−0.055	1.2 x 0.4
N13	0.1	0.35	10^{-4}	10^{-6}	10^{-7}	3000	−0.074	***1.6 x 0.3***
N14	0.1	0.35	10^{-4}	10^{-6}	10^{-7}	3000	−0.037	***0.8 x 0.6***
N15	0.1	0.35	10^{-4}	10^{-6}	10^{-7}	3000	***−0.037***	1.2 x 0.4
N16	0.1	0.35	10^{-4}	10^{-6}	10^{-7}	3000	***−0.074***	1.2 x 0.4
N17	0.1	0.35	10^{-4}	10^{-6}	10^{-7}	3000	***−0.110***	1.2 x 0.4
N18	0.1	0.35	10^{-4}	10^{-6}	10^{-7}	***6000***	−0.110	2.4 x 0.4
N19	0.1	0.35	10^{-4}	10^{-6}	10^{-7}	***12,000***	−0.220	4.8 x 0.4

4.1. Reference model and repeatability

In the reference model, the values of the frictional and mechanical parameters are based on the literature as much as possible. The friction coefficient between carbon fibres was chosen as$\mu_{ff} = 0.1$ based on the experiment by Tabor [16]. The friction coefficient between the fibres and the glass was fixed at $\mu_{fgl} = 0.35$, as this value is an average of the experimental friction coefficients measured in this and our previous experiments [28]. The torsional and bending stiffnesses are fixed based on the mechanical calculations presented earlier. The box with the same distribution of fibre diameters was generated three times, and the simulation of one sliding cycle was repeated to evaluate repeatability.

The images of the reference model at different moments of sliding are presented in Fig. 5. In the initial configuration, shown in Fig. 5 (a), one can see the rectangular box filled with fibres and the voids created by the ghost particles. The second image in Fig. 5 (b) illustrates the tow just after the end of compression. The absolute vertical reaction of the upper plate is slightly higher than that of the bottom plate due to a slight tilt of the upper plate and the bending resistance of the fibres. The rotation is not restricted, and as the load is applied at the center of the plate, which is shifted to the left with respect to the tow, a slight inclination of the plate is observed (consistent with experimental results). In the third image, Fig. 5 (c), the tow is shown just after the end of the forward sliding pass. The colour scale represents the horizontal displacement of the particles and the plates. The scale is saturated at 0.15 mm to highlight the displacements of the individual particles. A closer look at the image reveals that a layer of particles right under the sliding glass plate has a higher displacement values compared to other particles. The fibres in this layer are partially adhered to the glass plate due to a higher friction coefficient between glass and carbon fibre ($\mu_{fgl} =$ 0.35) than that between carbon fibers (μ_ff = 0.1), and due to the allowed rotation, which creates rolling. Fig. 5 (c) shows that while most of the particles have not rolled significantly, some of them, especially in the top and bottom layers in contact with the plates, rotated by up to + 4 and −16 rad. The high torsional angles experienced by the fibres are not surprising because of their long length and small torsional stiffness (Eq. (2). The last image in Fig. 5 illustrates the final state of the tow after 5.5 s of compression and forward and backward sliding. One can notice that the shear of the tow is in the opposite direction compared to the state after the forward sliding. The horizontal displacement of most of the particles is negative, and the top layer is distinguished again.

To compare the results of different models, three parameters were chosen and calculated at the end of each pass during the first sliding cycle similarly to the experiment. The friction coefficient between the tow and the sliding glass plate μ_T was calculated as the ratio of the horizontal and vertical reaction forces of the sliding glass plate. The displacement d_T and the strain ε_T are also calculated at each time step using the same method as in the experiments. The values extracted at the end of each pass as well as the friction coefficient averaged on the last 50 % of sliding of the numerical and experimental results are presented in Table 2.

The results of simulations N1, N2 and N3, as presented in Table 2 and Fig. 6, exhibit variability in behavior across the three repetitions. To determine whether this variability arises from different arrangements of the fibres in the initial model, the simulation was repeated using the exact same initial tow. The variability observed between these two results closely resembles that seen among simulations N1, N2 and N3, as illustrated in Fig. 6. This similarity can be partially attributed to numerical truncation errors, which contribute to the displacements of the numerous particles involved.

However, it is essential to understand the stochastic nature of both the model and, to some extent, the real tow. Due to the large voids present in the initial configuration of the tow (as shown in Fig. 5 (a)) and the significant displacements of the particles during compression, a variety of configurations can emerge after compression and before sliding, all stemming from the same initial setup. Consequently, some degree of variability in the behaviour of this system is inevitable.

The friction coefficient in simulations, 0.3 and 0.25 on average of three repetitions, is lower than the one measured experimentally, 0.38 and 0.33 respectively in forward and backward passes. However, the difference between the forward and backward friction coefficients is similar in both simulations and experiments. It is interesting to note that the friction coefficient between the tow and the sliding glass plate μ_T calculated from the simulations is different from the friction coefficient between the carbon fibre and the glass $\mu_{fgl} = 0.35$ used as an input parameter. The instantaneous friction varies all over the cycle and presents similar features to the experimental curves shown in Fig. 2: the initial phase of progressive increase in friction and the stabilised phase with some oscillations from the average value. These phases were observed in our previous incremental friction experiments [28] and were explained as the shear phase and the macroslip phase. The results of the continuous experiments presented here confirm this interpretation.

The friction increases gradually on the first 0.1 mm, which corresponds to a high gradient in the strain of the tow. The displacement must be non-zero mostly due to its definition: the geometrical centre of the

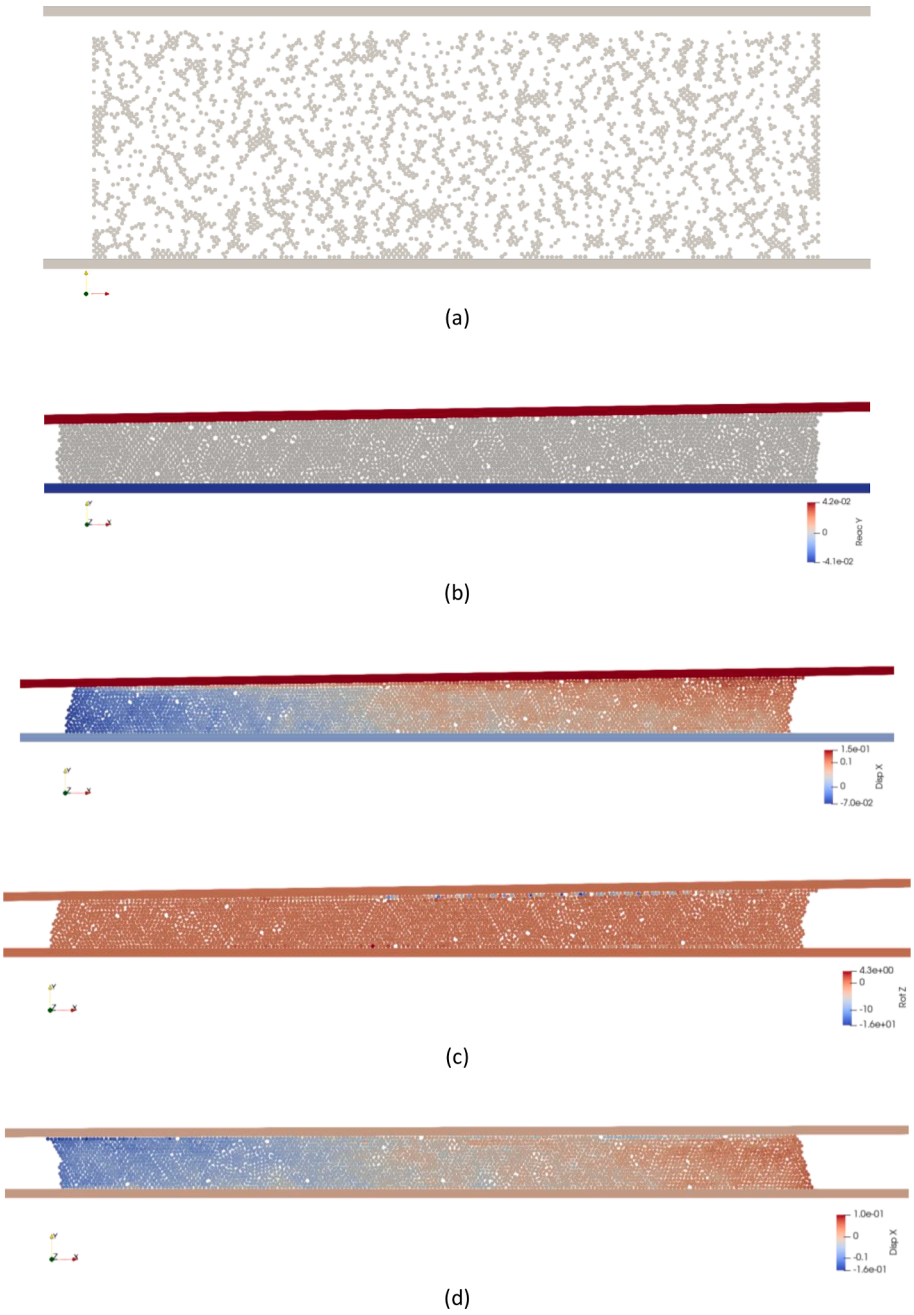

Fig. 5. Reference model at several time steps of the simulation with different colour scales: (a) 0 s initial geometry, (b) 1 s vertical reaction highlighted, (c) 3.5 s horizontal displacements and rotation of the particles highlighted and (d) 5.5 s horizontal displacement highlighted.

tow moves with the changes of its area due to stretch or contraction. The same behaviour is observed in Fig. 2 on experimental curves. Although the dispersion between the tows is obvious, the friction coefficient of all of them seem to stabilise close to the point of the end of the rapid increase of the strain.

Once the shear of the tow reached its mechanical limit, the macroslip of the tow/glass interface starts and the friction coefficient stabilises. This shear limit is a balance between the bending behaviour of individual fibres, conditioned by the axial force in each fibre, and the friction force. From that point, the displacement increases continuously, but the increase in strain is less pronounced than in the first stage.

It is not possible to compare quantitatively the values of strain and displacement with the experiment since there are only 3000 fibres in the model compared to the 12,000 fibres in the real tow. The compacity of the tow plays a significant role as well. It is clear that real fibres are not all well aligned, parallel and straight, which creates voids in a cross section of the tow and a variation of bending stiffness. This cannot be represented in the two-dimensional DEM model. Nevertheless, the experimental and numerical results are qualitatively similar: the displacement in a cycle is an open loop with a negative residual displacement at the end, and the strain increases during the forward sliding and remains rather stable on the backward pass.

4.2. *Influence of local friction coefficients*

In this section, the global sliding behavior of the tow with respect to local frictional coefficients between fibres μ_{ff} and between fibre and glass μ_{fgl} will be discussed.

The simulations N4 and N5 assume that the friction coefficient between fibres is not 0.1 but 0.3 and 0.5 respectively. The results presented

Table 2
Results of the simulations and the experiments of one cycle sliding.

Simulation	Friction coefficient μ_T		Displacement at the end of the pass d_T, mm		Strain at the end of the pass ε_T	
	Forward	Backward	Forward	Backward	Forward	Backward
N1 (Ref)	0.290	0.274	0.045	−0.021	0.098	0.102
N2	0.318	0.244	0.048	−0.024	0.082	0.095
N3	0.281	0.229	0.055	−0.020	0.096	0.082
N4	0.204	0.142	0.053	−0.019	0.080	0.086
N5	0.259	0.187	0.052	−0.017	0.089	0.097
N6	0.281	0.234	0.050	−0.019	0.092	0.092
N7	0.282	0.233	0.055	−0.020	0.112	0.103
N8	0.263	0.221	0.069	−0.003	0.065	0.069
N9	0.365	0.349	0.045	−0.035	0.085	0.127
N10	0.357	0.343	0.028	−0.016	0.053	0.073
N11	0.291	0.214	0.155	−0.064	0.262	0.345
N12	0.316	0.231	0.077	−0.024	0.089	0.082
N13	0.280	0.206	0.037	−0.035	0.053	0.083
N14	0.298	0.257	0.096	−0.020	0.105	0.093
N15	0.314	0.261	0.044	−0.019	0.064	0.078
N16	0.280	0.242	0.066	−0.026	0.082	0.113
N17	0.281	0.211	0.074	−0.027	0.119	0.138
N18	0.292	0.266	0.038	−0.029	0.038	0.041
N19	0.253	0.242	0.026	−0.025	0.010	0.010
Experiment	0.376 ± 0.036	0.335 ± 0.019	0.581 ± 0.149	−0.415 ± 0.155	0.070 ± 0.015	0.037 ± 0.029

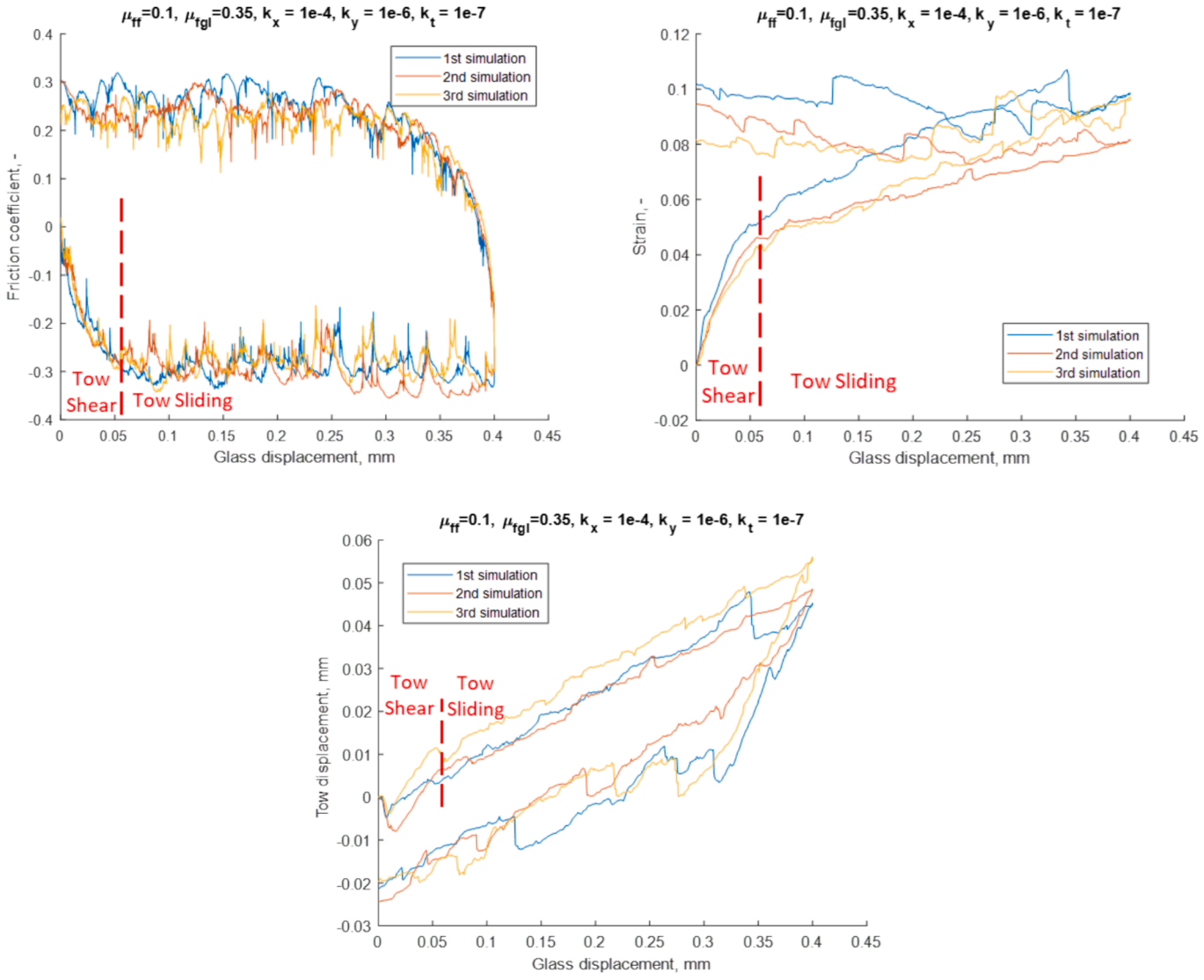

Fig. 6. Results of three repeated simulations on the reference model with different initial configurations.

in Table 2 demonstrate that this parameter has an impact on the global friction coefficient μ_T. In both simulations, this coefficient is lower than in the reference configuration, but the tendency is not monotonic. On the contrary, there is no difference in displacement and strain of the tow when the friction coefficient between fibres is changed. It could be explained by the higher loss of frictional energy inside the tow which results in smaller friction loss at the interface with the glass plate. The number of fibres in contacts with the glass plate is lower with higher μ_{ff}. It is on average 185 for N1, 175 for N4 and 165 for N5 during the last 50 % of the forward sliding pass.

The effect of fibre/glass friction coefficient on the tow coefficient was tested in simulations N6 and N7. The values of 0.5 and 0.7 for μ_{fgl} compared to 0.35 in the reference simulation were chosen. The results of these simulations presented in Table 2 are surprising. They show that there is no effect of the fibre/glass friction coefficient neither on the global friction of the tow μ_T, nor on its displacement and strain.

These results reveal that the friction measured between the tow and the sliding plate is a combination of both fibre/fibre and fibre/glass friction. If the fibre/glass friction is significantly higher than the fibre/fibre friction as in simulations N1, N6 and N7, the global friction is governed mostly by the fibre/fibre value since the top layer of fibres is partially stuck to the plate. The value of the fibre/glass friction coefficient is not important. If, on the opposite, the fibre/glass friction is lower than the fibre/fibre friction as in N5 or close to it as in N4, the global friction is lower probably due to easier sliding and rolling of the fibres on the glass.

4.3. Influence of bending and torsional stiffness of the fibres

The simulations N8, N9 and N10 explore the differences in the behaviour of the tow when the torsional stiffness of the fibres is different from the reference value of 10^{-7}N mm. This value is estimated with very strong hypotheses; therefore, it can easily be at least one order of magnitude higher or lower. A simulation with restricted rotation of the fibres, N10, was also tested. The results presented in Table 2 and Fig. 7 show the great significance of this parameter in the sliding behaviour of the tow.

The average friction coefficient of the tow/glass interface changes from 0.26 to 0.36 when the torsional stiffness of the fibres varies between 10^{-8} and 10^{-6}N mm. The frictional curve with the higher torsional stiffness is flat by portions meaning that fibres do not move with glass, which is also revealed by the plateaux on the tow strain and displacement graphs. With infinite torsional stiffness, after the initial shear phase, the sliding is almost smooth with few spikes in friction coefficient corresponding to sudden changes of strain and displacement.

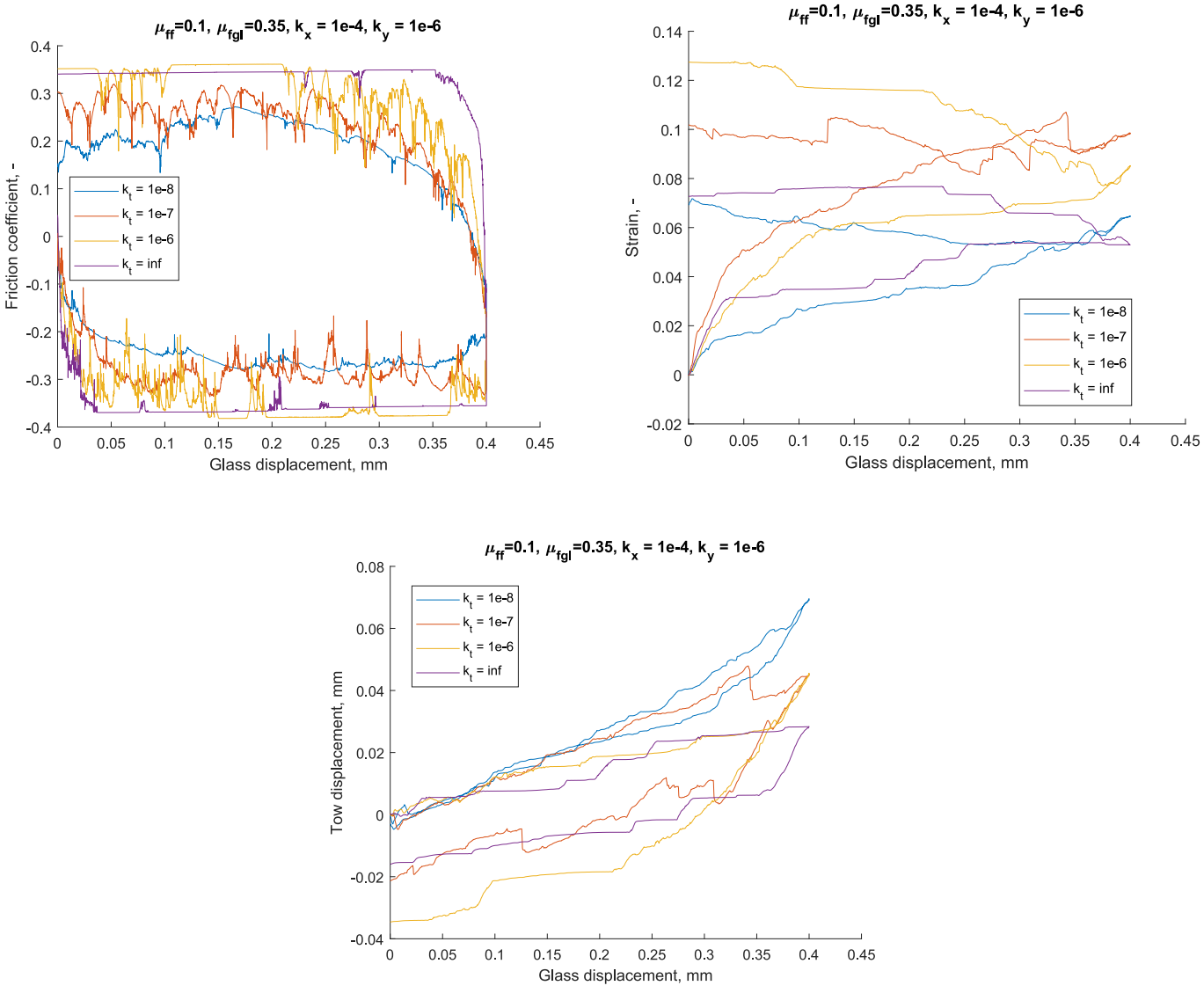

Fig. 7. Effect of torsional stiffness on tow sliding behaviour.

It is also interesting to note that when the torsional stiffness is low, the tow displacement is the highest and presents no hysteresis between the forward and backward sliding. However, the strain is very similar between low and infinite torsional stiffness since it is related mostly to local events seen as drops in friction and corresponding to rapid rearrangements of fibres.

Simulations N11 and N12 explore the effect of the linear bending stiffness of the fibres. The values of 10^{-4} and 10^{-5}N mm^{-1} have been tested for vertical and horizontal stiffness. The results show that this parameter has no impact on the average frictional coefficient of the tow. However, the displacement and strain increase significantly in simulation N11 when the horizontal stiffness is 10 times lower than in the reference configuration. The impact of the vertical linear stiffness (N12) on these parameters is very limited. Despite its limited impact, the vertical stiffness should not be too high since it is responsible for the compression step during the first second. If it is high, the particles are attracted not realistically to their initial position above the glass plate during sliding.

The results presented in this paragraph highlight the high importance of the torsional stiffness and horizontal linear stiffness of the fibres for the sliding behaviour of the tow. The influence of mechanical parameters of the fibres is significantly higher than that of their individual frictional coefficients. This holds for the average friction coefficient of tow, its strain and also its displacement. In the next paragraphs, the impact of the initial tow shape and of normal load will be studied.

4.4. Influence of the shape of the tow

In this section, the initial width and height of the rectangular box filled with particles are changed to study its impact on the results. The number of fibres is kept constant and the value of the normal load is adjusted for each simulation depending on the width of the tow to have the same normal pressure. The initial position of the top glass plate is also adjusted with respect to the centre of gravity of the tow. The boxes with the initial width of 2/3 and 4/3 of the reference value are studied in simulations N13 and N14. Since the number of fibres is constant, the thicknesses of the initial box are 600 μm and 300 μm respectively. After compression, the tow was 155 μm in the first case and only 84 μm in the second. The results of these simulations, presented in Table 2 and in Fig. 8, shows that the shape of the tow has an impact on all three parameters and their evolution during the sliding cycle.

When the tow is narrow and thick, as in simulation N14, the sliding glass plate's initial tilt is higher than in other cases because its centre of gravity is closer to the end of the tow. During sliding, the glass plate goes

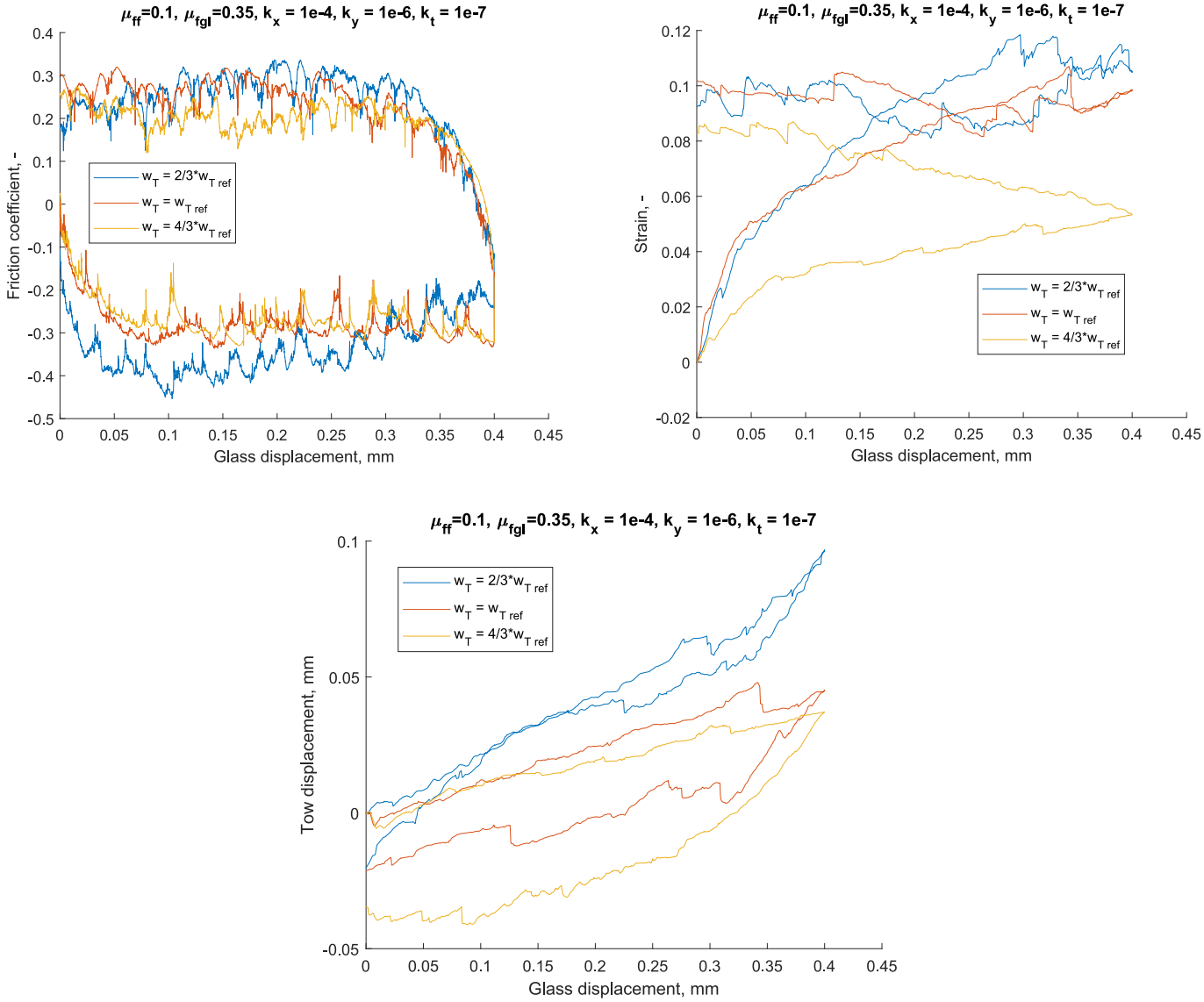

Fig. 8. Effect of the shape of the tow.

over the tow and the tilt inverses the sign. This is visible on the frictional curve, which is not flat as the other two curves presented in the same figure. However, the friction coefficient of this test is similar on average to the reference configuration as can be seen in Table 2. Although the strain behaviour is similar between the narrow and the reference tow, the displacement of the narrower tow is higher and does not present any hysteresis. This means that there is no delay between the forward and backward sliding of the tow. On the other hand, the wider tow presents higher hysteresis in sliding and lower strain levels. But the strain increases almost linearly after the initial shear despite the change in sliding direction at the end of the first pass.

4.5. Influence of the normal load

Normal (compression) load is the parameter that can be adjusted in forming processes. In this section, its effect on the sliding behaviour of the tow is examined. The simulations N15, N16 and N17 use the values of normal load 2/3, 4/3 and 2 times the reference normal load distributed over the same width of the tow. The results in Table 2 indicate that there is no significant effect on the friction of the tow, but the strain and tow displacement increase with normal load.

4.6. Influence of the number of fibres

Finally, two last simulations, N18 and N19 are meant to explore the scale effect of the model on the behaviour of the tow. The number of fibres is 6000 in the N18 simulation and 12,000 in the N19 simulation. Normal load, maximal displacement of the glass, its sliding speed and its width are also scaled, while the individual friction coefficients and the stiffness parameters of the fibres are kept constant. The thickness of the tow is identical to the reference configuration, while its width is 2 and 4 times higher. The results are presented in Fig. 9 and Table 2.

The curves presented in Fig. 9 show that the maximal displacement of the tow and, even more significantly, its strain are the highest for the tow of 3000 fibres and decrease with the number of fibres. This is similar to the effect of the width of the tow explored previously. Tow strain is actually a movement of individual fibres, which are restrained by the same bending stiffness in small and large models. The same displacements of fibres create lower strain for the larger tow than for the narrower one since it is normalized by the initial width of the tow. The internal friction must play a role as well since the global displacement of the tow is also affected by the number of fibres, but to a lesser extent. The stabilised friction between the sliding glass plate and the tow is similar on average between 3000 and 6000 fibres models, but it is lower for the 12,000 fibres model. The significant difference between these

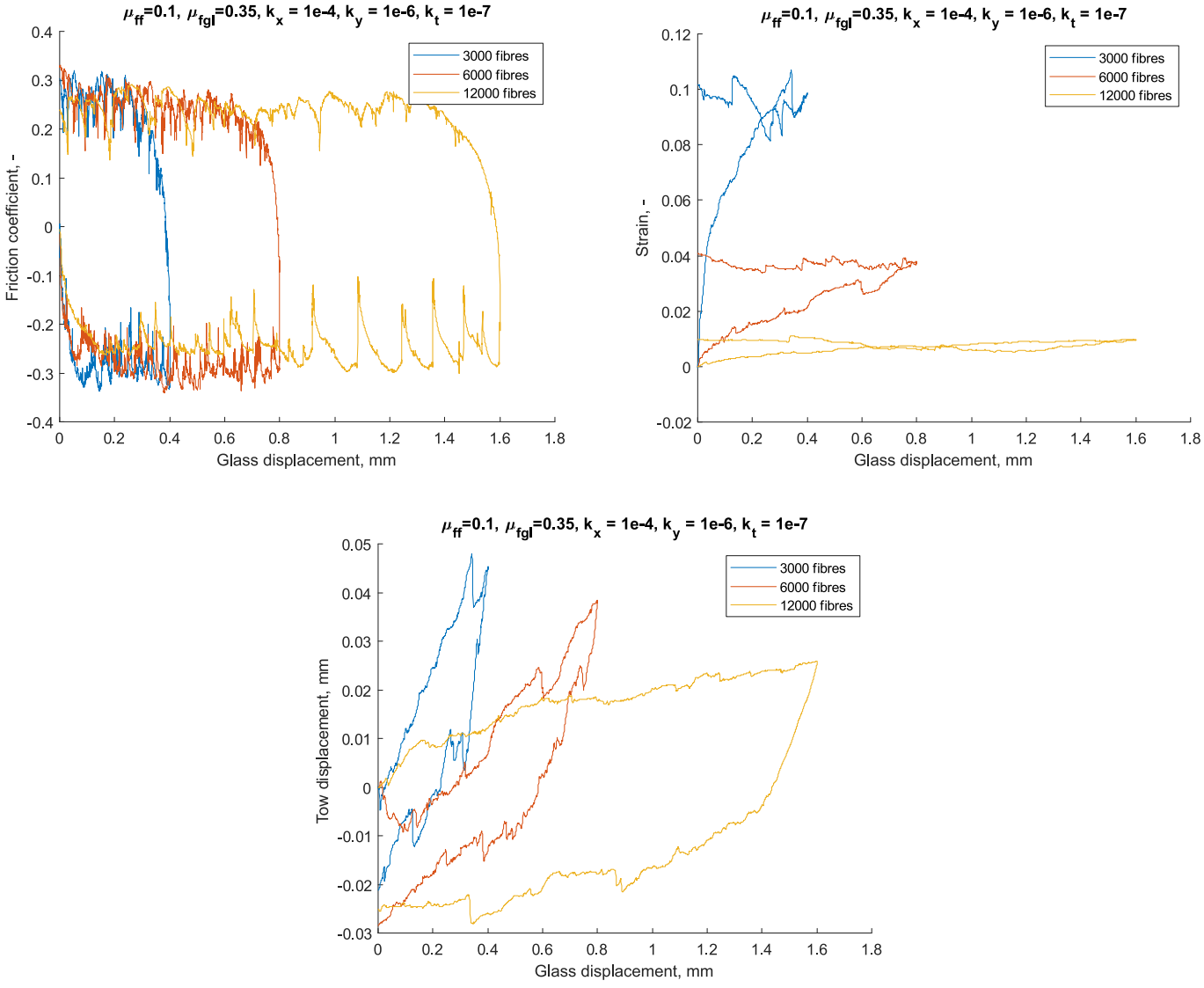

Fig. 9. Effect of the number of fibres.

models resides in the length of the initial shear phase, which is shorter for a smaller number of particles both in the forward and backward sliding.

4.7. Cyclic response of the reference model versus experiment

It is likely that during forming processes, tows slide repeatedly in different orientations either accidentally or on purpose. In the presented experiment, it is also possible that during the manual handling of the tows and the setup of the experiment, there was some sliding before the recorded data. The effect of repeated sliding is explored in this section both with simulations and experiments.

Four forward and backward sliding cycles were simulated on the models N1 and N2 with similar parameters and different particle deposition. A holding phase of 0.5 s was introduced after each sliding pass, so the cycles start at 0 s, 5 s, 10 s and 15 s. The results presented in Fig. 10 are to be compared qualitatively with the experimental results presented in Fig. 11. The simulated curves reveal that there is some, rather limited, variability between the resulting curves of four cycles in friction coefficient and displacement of the tow. There is also a small difference between the two simulations, in the same range as observed previously in Fig. 6. However, the strain behaviour of the first cycle is completely different from the further cycles in both simulations. There is a significant positive strain during the first sliding pass, which stays rather constant during the backward sliding. In the second cycle, a small increase in strain during sliding forward is reversed during the backward sliding. From the third cycle, the strain behaviour seems to stabilize with an amplitude of 0.02 reversible after each cycle.

During longer experiments, the frequency of the capture of microscopic images appeared not to be constant. Therefore, to improve the readability of the figure, the time scale of the displacement and strain curves presented in Fig. 11 was scaled to coincide the end of the sliding cycles with the friction signal which was measured with high frequency and accuracy. The four tests differed also in the time of break between the sliding passes, but this parameter did not have any significant influence on the results. These curves demonstrate highly dispersed

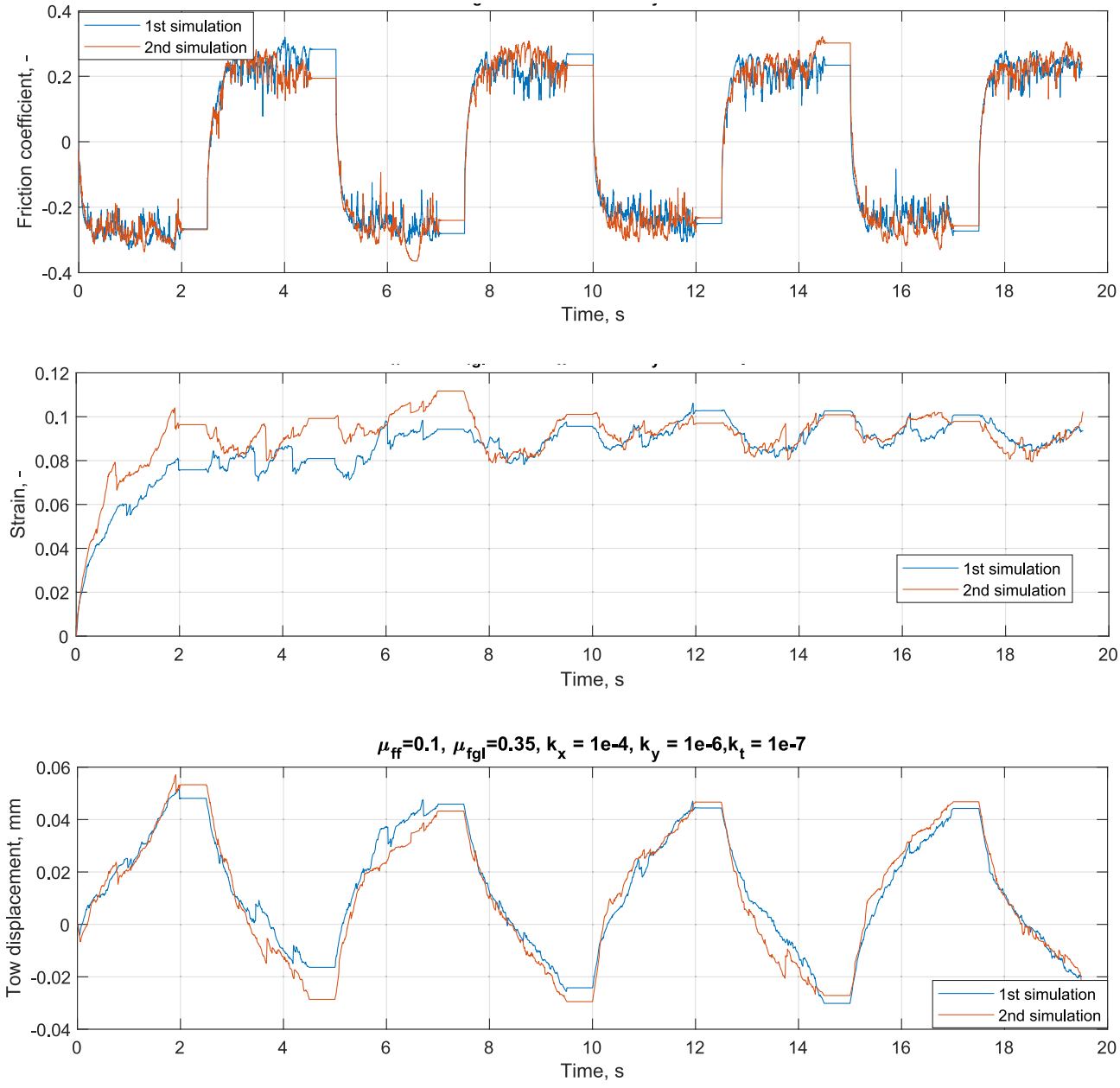

Fig. 10. Simulated response of four cycles of sliding on the models N1 and N2.

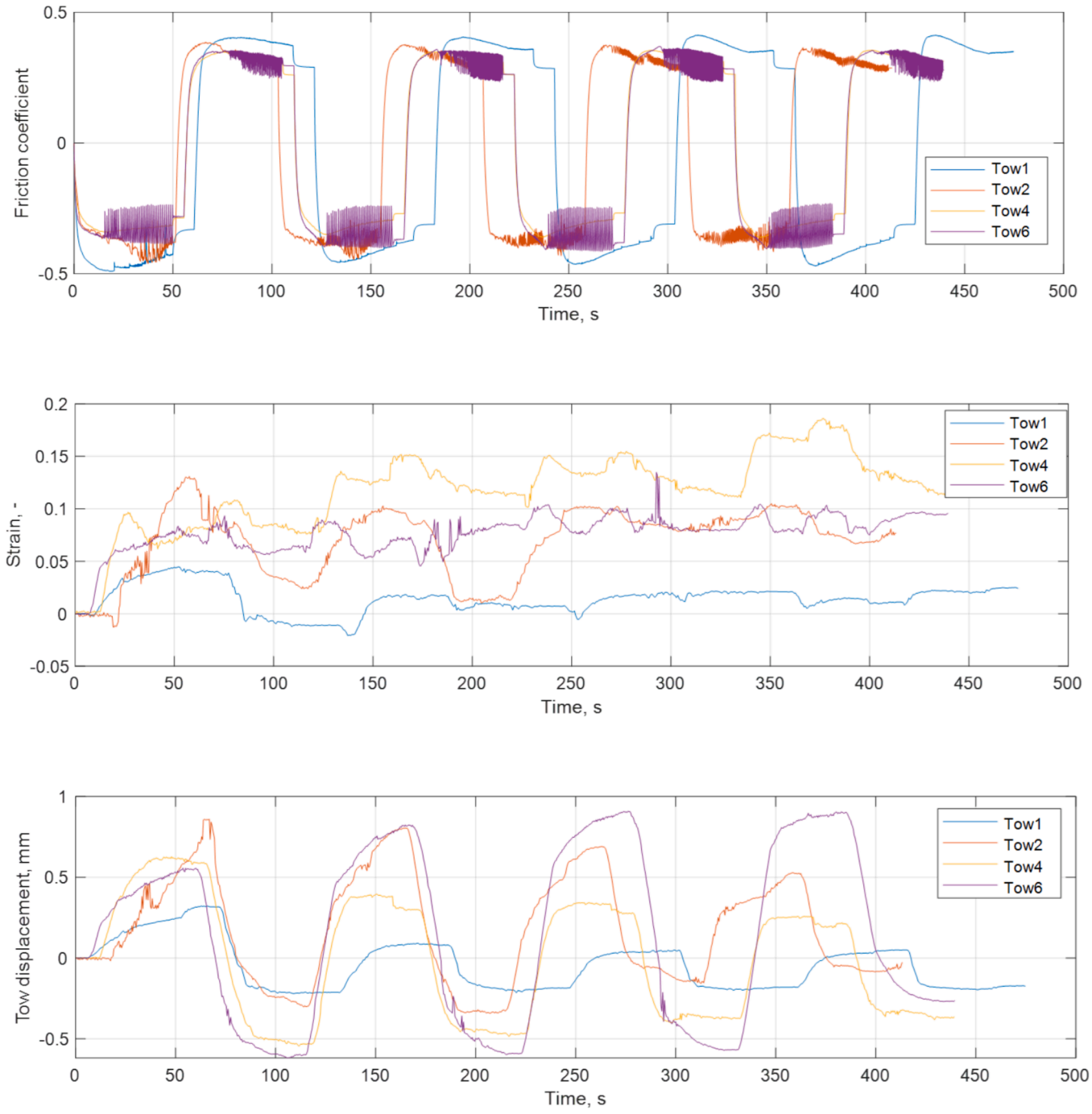

Fig. 11. Experimental response of four tows during four sliding cycles.

behaviour between the four tows, similarly to Fig. 2 presented previously. Although the friction curves seem stabilised after the first cycle and similar between the four tows, the displacement and strain behaviour continue to change during the cycling, but seem to tend to some stabilization as well. However, this stabilised level of strain and displacement amplitude is different for each tow. The simulations carried out in previous paragraphs can explain now these discrepancies by the initial width of the tow, axial tensile force in the fibres and unintentional sliding previous to measurement. As mentioned before, the width of four tows varied between 6.5 and 8.8 mm which corresponds to the ratio of 4/3 that was explored in Fig. 8. The effect on the strain revealed by the simulations was significant. The variations of axial tension force in 12,000 fibres cannot be measured unfortunately and the difference between the tows remains a hypothesis. After analysis of the numerical results of the cyclic tests, it is possible to suggest that the first cycle of sliding for Tow 1 presented in Fig. 11 was not actually the first, because its strain curve looks more like the one from the simulations starting from the 2nd cycle.

5. Conclusions

A frictional experiment on a dry carbon fibre tow in transversal to fibre orientation sliding direction was carried out on four pieces of tow cut from the same spool. A specially developed experimental setup enables simultaneous measurement of friction force and observation of the tow through a glass window sliding on its surface. The microscopic

images are analysed to calculate the displacement of the tow centre and the transversal strain, both induced by the sliding of the glass plate under compression load. The results show high dispersity in these three signals for four tested tows. Despite the axial tension load applied on the tow before clamping it at both ends, the displacement and strain are non-negligible, which evidences displacements of individual fibres.

To understand this behaviour, a two-dimensional discrete element model of the tow and glass plates, representative of the experiment, is created. The sliding behaviour of the tow is conditioned by four parameters: two structural parameters, the bending and torsional stiffness of the fibres, and two frictional parameters, the friction coefficient between two fibres and the friction coefficient between fibre and glass. Former parameters are dependent on the axial tension in the fibres and the latter ones are seen as material parameters, independent of the structure. These coefficients are a priori unknown, especially since the axial tension in fibres is very likely to differ between 12,000 fibres composing the tow. A parametric analysis was then performed to evaluate the impact of each of these parameters. The conclusions can be summarized as

- Two phases of sliding, shear of the tow and actual sliding, suggested in our previous paper [28] were clearly distinguished in numerical results. The extent of the shear phase is dependent on the number of the fibres and the shape of the tow.
- The model with exactly the same parameters and the same set of fibres run three times with different arrangements of the fibres in the tow gave some variability in the results (at least 10 %).
- The frictional coefficients between fibres and fibres and glass have a limited effect on the sliding behaviour of the tow. When the fibre/glass coefficient is higher than the fibre/fibre coefficient, its actual value has no impact at all on the results. When the fibre/fibre coefficient is close to or higher than the fibre/glass coefficient, the apparent friction coefficient between the tow and the sliding glass plate changes significantly due to a separation of the tow into two layers sliding one on top of another.
- The structural parameters are found to be the most significant in this study and especially torsional stiffness. If fibres are free to roll, friction and strain of the tow decrease drastically, while its displacement increases in the same proportion. On the contrary, when the rotations are restrained, the friction signal is high and almost constant during sliding, only changes in displacement and strain are due to local instabilities of some fibres.
- Bending stiffness has a small impact on the friction when fibre can roll, but conditions the displacement and the strain of tow.

After this parametric study, the impact of normal load, shape of the tow and number of fibres was studied to provide useful guidance for forming optimisation. It was found that the normal load does not have a significant effect on the friction of the tow, but the strain and tow displacement increase with the normal load. A narrower tow presents higher displacement than the wider one under the same load, it is more mobile and responds quickly to the change of sliding direction. When comparing the response of 3000, 6000 and 12,000 fibres models, it is necessary to remember that the sliding behaviour of the tow is the combination of the sliding behaviour of its fibres, which are conditioned by the stiffness and local frictional parameters of each one. Thus, with the same structural and frictional parameters, the model of 12,000 fibres moves and deforms significantly less than the two other models. The friction is less affected except for the shear phase, which is dependent on the ratio between the thickness and the width of the tow.

Finally, four cycles of sliding were simulated and compared with four cycles performed on the experimental setup. While, the simulations revealed similarities of friction and displacement curves between the four cycles, the increase of strain during the first sliding pass was significantly higher than the further cycles. The strain behaviour stabilised after the second cycle due to the accommodation of the tow. Based on these numerical results, the high dispersity in experimental results is explained by differences in the initial width of the tow, tensile force in the fibres and unintentional sliding prior to measurement. Overall, the tendencies in experimental and numerical results are rather similar.

The results of this paper are believed to be highly significant for understanding and preventing sliding-induced deformations of the tows during composite fabric forming processes. By optimising the parameters cited above, it is possible to minimize the sliding defects and control the friction for the fabric from any nature of fibre. It needs to be emphasised though that the fibres used in this work have circular cross-sections, thus it would be necessary to test fibres of less perfect shape in future work.

Above all, the Discrete Element Method proved itself to be a very interesting and powerful tool to investigate the friction problems of composite materials during manufacturing due to the possibility to handle a high number of fibres with a low computation cost. The model can be easily adapted to other types of processes with different contact geometries and boundary conditions. A possibility of extension of the model to three dimensions exists [37], but it comes with an increase in computational cost.

CRediT authorship contribution statement

Olga Smerdova: Writing – review & editing, Writing – original draft, Visualization, Validation, Supervision, Software, Resources, Project administration, Methodology, Investigation, Funding acquisition, Formal analysis, Data curation, Conceptualization. **Chenghao Chai:** Investigation, Formal analysis, Data curation. **Ismail Kolimi:** Investigation, Formal analysis, Data curation. **Noël Brunetière:** Writing – review & editing, Validation, Supervision, Methodology, Investigation, Funding acquisition, Conceptualization.

Declaration of competing interest

The authors declare that they have no known competing financial interests or personal relationships that could have appeared to influence the work reported in this paper.

Acknowledgments

The authors are grateful to Dr M. Renouf, Dr F. Dubois and R. Mozul for advice about LMGC90 software and to Dr M. Gueguen for help with the use of the supercomputer facilities of the Mesocentre. This work pertains to the program “Investissements d’Avenir” (ANR-11-LABX-0017-01 and ANR-18-EURE-0010). Pprime Institute gratefully acknowledges “CPER” Nouvelle Aquitaine as well as the “FEDER” for their financial support.

Data availability

Data will be made available on request.

References

[1] Lunetto V, Galati M, Settineri L, Iuliano L. Sustainability in the manufacturing of composite materials: a literature review and directions for future research. J Manuf Proc 2023;85:858–74. https://doi.org/10.1016/j.jmapro.2022.12.020.
[2] Bourban PE, Bernet N, Zanetto JE, Månson JAE. Material phenomena controlling rapid processing of thermoplastic composites. Compos. Part A: Appl. Sci. Manuf. 2001;32(8):1045–57. https://doi.org/10.1016/S1359-835X(01)00017-3.
[3] van Rijswijk K, Bersee HEN. Reactive processing of textile fiber-reinforced thermoplastic composites – an overview. Compos. A Appl. Sci. Manuf. 2007;38:666–81. https://doi.org/10.1016/j.compositesa.2006.05.007.
[4] Ageyeva T, Sibikin I, Kovács JB. A review of thermoplastic resin transfer molding: process modelling and simulation. Polymers 2019;11(10):1555. https://doi.org/10.3390/polym11101555.
[5] Fetfatsidis KA, Jauffrès D, Sherwood JA, Chen J. Characterization of the tool/fabric and fabric/fabric friction for woven-fabric composites during the thermostamping

process. Int. J. Mater. Form. 2013;6:209–21. https://doi.org/10.1007/s12289-011-1072-5.
[6] Gorczyca-Cole JL, Sherwood JA, Chen J. A friction model for thermostamping commingled glass–polypropylene woven fabrics. Compos. A Appl. Sci. Manuf. 2007;38:393–406. https://doi.org/10.1016/j.compositesa.2006.03.006.
[7] Sachs U, Akkerman R, Fetfatsidis K, Vidal-Salle E, Schumacher J, Ziegmann G, et al. Characterization of the dynamic friction of woven fabrics: experimental methods and benchmark results. Compos. A Appl. Sci. Manuf. 2014;67:289–98. https://doi.org/10.1016/j.compositesa.2014.08.026.
[8] Das A, Choong GYH, Dillard DA, De Focatiis DSA, Bortner MJ. Characterizing friction for fiber reinforced composites manufacturing: method development and effect of process parameters. Compos. B Eng. 2022;236:109777. https://doi.org/10.1016/j.compositesb.2022.109777.
[9] Cornelissen B, Rietman B, Akkerman R. Frictional behaviour of high performance fibrous tows: friction experiments. Compos. A Appl. Sci. Manuf. 2013;44:95–104. https://doi.org/10.1016/j.compositesa.2012.08.024.
[10] Smerdova O, Sutcliffe MPF. Novel experimental method for microscale contact analysis in composite fabric forming. Exp. Mech. 2015;55(8):1475–83. https://doi.org/10.1007/s11340-015-0044-y.
[11] Smerdova O, Sutcliffe MPF. Multiscale tool–fabric contact observation and analysis for composite fabric forming. Compos. A Appl. Sci. Manuf. 2015;73:116–24. https://doi.org/10.1016/j.compositesa.2015.03.009.
[12] Mulvihill DM, Smerdova O, Sutcliffe MPF. Friction of carbon fibre tows. Composites 2017;93:185–98. https://doi.org/10.1016/j.compositesa.2016.08.034.
[13] Mulvihill DM, Sutcliffe MPF. Effect of tool surface topography on friction with carbon fibre tows for composite fabric forming. Compos. A Appl. Sci. Manuf. 2017;93:199–206. https://doi.org/10.1016/j.compositesa.2016.10.017.
[14] Chakladar ND, Mandal P, Potluri P. Effects of inter-tow angle and tow size on carbon fibre friction. Compos. A Appl. Sci. Manuf. 2014;65:115–24. https://doi.org/10.1016/j.compositesa.2014.06.002.
[15] Tourlonias M, Bueno M-A, Fassi G, Aktas I, Wielhorski Y. Influence of friction angle between carbon single fibres and tows: experimental analysis and analytical model. Compos. A Appl. Sci. Manuf. 2019;124:105478. https://doi.org/10.1016/j.compositesa.2019.105478.
[16] Roselman IC, Tabor D. The friction of carbon fibres. J. Phys. D Appl. Phys. 1976;9(17):2517. https://doi.org/10.1088/0022-3727/9/17/012.
[17] Tourlonias M, Bueno M-A, Poquillon D. Friction of carbon tows and fine single fibres. Compos. A Appl. Sci. Manuf. 2017;98:116–23. https://doi.org/10.1016/j.compositesa.2017.03.017.
[18] Tourlonias M, Bueno M-A, Jordan C, Poquillon D. Influence of wear on the sizing layer and desizing of single carbon fibre-to-fibre friction. Wear 2018:40264–370. https://doi.org/10.1016/j.wear.2018.02.003.
[19] Sugimoto Y, Shimamoto D, Hotta Y. Evaluation of kinetic friction coefficients between single carbon fibers. Carbon 2020;167:264–9. https://doi.org/10.1016/j.carbon.2020.06.010.
[20] Potter K, Khan B, Wisnom M, Bell T, Stevens J. Variability, fibre waviness and misalignment in the determination of the properties of composite materials and structures. Compos. A Appl. Sci. Manuf. 2008;39:1343–54. https://doi.org/10.1016/j.compositesa.2008.04.016.
[21] Hamidi YK, Altan MC. Process induced defects in liquid molding processes of composites. Intern Polymer Processing XXXII 2017:5. https://doi.org/10.3139/217.3444.
[22] Alves MP, Cimini CA, Ha S. Fiber waviness and its effect on the mechanical performance of fiber reinforced polymer composites: an enhanced review. Compos. A Appl. Sci. Manuf. 2021;149:106526. https://doi.org/10.1016/j.compositesa.2021.106526.
[23] Viisainen JV, Sutcliffe MPF. Characterising the variability in wrinkling during the preforming of non-crimp fabrics. Compos. A Appl. Sci. Manuf. 2021;149:106536. https://doi.org/10.1016/j.compositesa.2021.106536.
[24] Guzman-Maldonado E, Wang P, Hamila N, Boisse P. Experimental and numerical analysis of wrinkling during forming of multi-layered textile composites. Compos. Struct. 2019;208:213–23. https://doi.org/10.1016/j.compstruct.2018.10.018.
[25] Boisse P, Huang J, Guzman-Maldonado E. Analysis and modeling of wrinkling in composite forming. J Compos Sci 2021;5:81. https://doi.org/10.3390/jcs5030081.
[26] J.J. Moreau. Unilateral contact and dry friction in finite freedom dynamics, in Non Smooth Mechanics and Applications, CISM Courses and Lectures, 302 (1988) 1-82.
[27] Jean M. The non smooth contact dynamics method. Compt. Methods Appl. Math. Eng. 1999;177:235–57.
[28] Smerdova O, Benchekroun O, Brunetière N. Transversal friction of epoxy-lubricated and dry carbon tows: from initial stages to stabilised state. Compos. A Appl. Sci. Manuf. 2021;143:106263. https://doi.org/10.1016/j.compositesa.2020.106263.
[29] O. Smerdova, O. Benchekroun, N. Brunetière. Deformation due to sliding of single and woven carbon tows in dry and epoxy-lubricated conditions. Paper presented at ESAFORM 2021. 24th International Conference on Material Forming, Liège, Belgique. 2021 doi.
[30] Cundall PA, Strack ODL. A discrete numerical model for granular assemblies. Géotechnique 1979;29(1):47–65. https://doi.org/10.1680/geot.1979.29.1.47.
[31] M. Jebahi, D. André, I. Terreros, I. Iordanoff, Discrete Element Method to Model 3D Continuous Materials. ISBN:9781848217706, 2015 John Wiley & Sons, Inc. doi: 10.1002/9781119103042.
[32] Champagne M, Renouf M, Berthier Y. Modeling wear for heterogeneous bi-phasic materials using discrete elements approach. J. Tribol. 2014;136(2). https://doi.org/10.1115/1.4026053.
[33] F. Radjai, F. Dubois. Discrete-element modeling of granular materials. Wiley-Iste, 425 p., 2011, ISBN:978-1-84821-260-2.
[34] https://git-xen.lmgc.univ-montp2.fr/lmgc90 (accessed on 27 August 2024).
[35] Islam F, Joannès S, Bucknell S, Leray Y, Bunsell A, Laiarinandrasana L. Investigation of tensile strength and dimensional variation of T700 carbon fibres using an improved experimental setup. J. Reinf. Plast. Compos. 2020;39(3–4):144–62. https://doi.org/10.1177/0731684419873712.
[36] Sawada Y, Shindo A. Torsional properties of carbon fibers. Carbon 1992;30(4):619–29. https://doi.org/10.1016/0008-6223(92)90181-U.
[37] del Sorbo P, Girardot J, Dau F, Iordanoff I. Numerical investigations on a yarn structure at the microscale towards scale transition. Compos. Struct. 2018;183:489–98. https://doi.org/10.1016/j.compstruct.2017.05.018.